Korean J. Chem. Eng., 39(11), 3055-3066 (2022)
DOI: 10.1007/s11814-022-1184-2

pISSN: 0256-1115
eISSN: 1975-7220

Microbially induced calcium precipitation based anaerobic biosynthetic crystals for removal of F^- and Ca^{2+} in groundwater: Performance optimization, kinetics, and reactor operation

Zhenyu Zhai*,, Amjad Ali*,**,†, Junfeng Su*,**,†, Zhenle Hao*,**, Jiaran Liu*,**, and Zhao Wang*,****

*School of Environmental and Municipal Engineering, Xi'an University of Architecture and Technology, Xi'an 710055, China
**Shaanxi Key Laboratory of Environmental Engineering, Xi'an University of Architecture and Technology, Xi'an 710055, China

(*Received 7 February 2022 • Revised 17 May 2022 • Accepted 18 May 2022*)

Abstract−Anaerobic biosynthetic crystals (ANBC) were prepared based on microbially induced calcium precipitation (MICP) and their potential explored for groundwater defluoridation and decalcification. The preparation conditions of ANBC were optimized and the influence of key factors (initial fluoride ions (F^-) concentration, pH, and initial calcium ions (Ca^{2+}) concentration) on the crystals was investigated. During the operation of the reactor, at pH of 7.0, the hydraulic retention time (HRT) of 6 h, and Ca^{2+} concentration of 180 mg L^{-1}, a maximum removal efficiency reached 93.31%, while 66.20% of Ca^{2+} could be removed. The adsorption dynamics study showed that the adsorption of ANBC was most in line with the pseudo-second-order model. The stability of ANBC operation was studied and failure reaction showed that the crystals maintained a stable removal ability after 35 times of repeated use. Further studies found that this was attributed to the continuous growth and synthesis of the crystals. The defluoridation and decalcification mechanism was further explored by scanning electron microscopy (SEM), energy dispersive spectroscopy (EDS), and X-ray diffraction spectra (XRD). This study innovatively proposes a method for biosynthesis of crystals under anaerobic conditions based on MICP, which can efficiently and stably remove F^- and Ca^{2+} in groundwater, providing a valuable strategy for groundwater contaminant remediation and energy saving.

Keywords: Adsorption Dynamics, Anaerobic Biosynthetic Crystals, Decalcification Defluoridation, Groundwater

INTRODUCTION

The deterioration of groundwater quality is a global issue. Fluoride (F^-) is one of the most commonly found contaminants in groundwater in various regions of the world [1,2]. The issue of F^- pollution has received critical attention due to its potential harm to human health and the environment [3]. In addition, the health risk assessment showed that long-term drinking of high F^- contaminated water (>3.0 mg L^{-1}) can pose a great threat to human health, such as skeletal fluorosis, dyspnea, tachycardia, severe gastroenteritis, and ventricular abnormalities, particularly in infants and children [4,5]. Furthermore, over-exploitation of land caused by anthropogenic activities increased F^- accumulation in groundwater [3]. The World Health Organization (WHO) has set 1.5 mg L^{-1} as the allowable limit for F^- concentration in drinking water [6] and China even stipulates that the value should not exceed 1.0 mg L^{-1}. However, the studies about F^- levels in natural water worldwide have shown an increasing trend in the concentration during the past 10 years [7]. Especially in Asia, the F^- concentration in groundwater has gradually exceeded 5 mg L^{-1} in many regions [8]. Therefore, it is urgent to find effective methods to deal with the problem of F^- pollution in groundwater.

Various conventional techniques have been reported on the removal of F^- in an aquatic environment, such as membrane, precipitation, and adsorption [9,10]. Among them, adsorption technology has been explored because of its high efficiency, simplicity, and economic viability [11,12]. Previous studies have suggested that adsorption technology has excellent performance in treating water with low contaminant concentrations [13]. There is no doubt that the application of this technology has great potential for the removal of F^- at low concentration in groundwater. However, most of the current adsorption materials used for F^- removal are complex to synthesize and the raw materials used may be potentially toxic, which is likely to cause secondary pollution to the environment [14,15].

Microbially induced calcium precipitation (MICP) is an environment-friendly technology that has been applied in the field of engineering [16,17]. This technique relies on the metabolism of the microbes by adjusting the physicochemical conditions of their environment to precipitate certain types of biomineral [18,19]. In the process of MICP, microorganisms serve as the nucleation sites and attract calcium ions (Ca^{2+}) to their surfaces through the negatively charged functional groups [20]. At the same time, CO_3^{2-} and HCO_3^- produced by microbial metabolism are released into the local environment and these ions react with Ca^{2+} to form precipitates [21]. In addition, Extracellular polymeric substances (EPS) produced by bacterial metabolism regulate crystal nucleation and promote the aggregation of crystals [22]. However, the operating cost largely restricts the application of this technology in real groundwater reme-

†To whom correspondence should be addressed.
E-mail: amjadali@aup.edu.pk, sjf1977518@sina.com

diation.

It is feasible to use precursor products (biosynthetic crystals) of MICP to repair groundwater [19]. As bioremediation, inducing crystallization has obvious advantages [23]. This method breaks the limitation of external organic matter, has a short reaction time, and does not produce tiny precipitates that are difficult to remove [24]. Considering the economic cost, the synthesis of crystals under anaerobic conditions has more advantages such as no additional aeration required, the process is simpler, and no other intervention is required, which greatly reduces energy consumption [25]. However, the research on anaerobic biosynthetic crystals (ANBC) is still quite limited and their adsorption properties for F^- demand further exploration. It is not clear whether it can be used as an ideal medium for F^- removal and has application potential in groundwater hardness. Therefore, it is worthy to conduct an evaluation study on ANBC.

In this study, we focused on the potential of ANBC in groundwater defluoridation and decalcification in an attempt to address the economic constraints of the practical application of MICP. The preparation conditions of the crystals were optimized, ANBC-based reactors were established, and the removal efficiencies of F^- and Ca^{2+} under different hydraulic retention time (HRT), pH, and initial Ca^{2+} concentration were explored. The adsorption kinetics experiment was used to study the adsorption process of ANBC, the long-term use performance of the crystals was explored, and its application stability was analyzed. Furthermore, ANBC was characterized by SEM, EDS, XRD, and its mechanism of action was explored.

MATERIALS AND METHODS

1. Preparation of ANBC and Optimization of Preparation Conditions

Cupriavidus sp. W12 has excellent autotrophic denitrification capability that helps in biomineralization, which was used in crystal synthesis in this study. ANBC was synthesized by culturing the strain W12 in an anaerobic bottle containing a heterotrophic medium (HM). Air tightened the cap and culture the anaerobic bottle in a thermostatic incubator at 30 °C. After 24 hours, the vacuum pump was used for filtration and the resulted precipitates were intercepted on the filter paper. Finally, ANBC were obtained by drying in an oven at 60 °C for 24 hours. The HM contains the following components (per liter): 1.0 g of $CaCl_2$ and $C_4H_4Na_2O_4{\cdot}6H_2O$, 0.2 g of KH_2PO_4 and $NaNO_3$, 0.10 g of $MgSO_4{\cdot}7H_2O$, and 2.0 mL of trace elements solution [26]. The chemicals used were analytical grade reagents, which were purchased from Aladdin Chemical Reagent Co., Ltd (China) and Tianjin Kemiou Chemical Reagent Co., Ltd (China). Sterile F^- reserve solution (1.0 mg mL^{-1}) was prepared by dissolving the solid NaF in sterilized distilled water to control the initial F^- concentration.

To determine the optimum medium for crystals preparation, the performance of crystals prepared under different concentrations of F^-, Ca^{2+}, PO_4^{3-}, and Mg^{2+} was studied, which was measured every two hours. The running effect of the crystals was determined under the optimal concentration of various substances. Subsequent experiments used crystals prepared at the concentration of optimal substances.

2. Adsorption Kinetics

Briefly, 1 L of groundwater was added to the conical flask, followed by 0.5 g of crystals and 0.5 g of $CaCl_2$ powder, and then 1.0 mg mL^{-1} concentrated sterile NaF reserve solution was added to adjust the F^- concentration to 1.0, 3.0, and 5.0 mg L^{-1}, after which the pH was adjusted to 7.0. The conical flasks were cultured statically at room temperature (25 °C) in an incubator. A total of eleven samples were taken between 1 and 12 h to determine the removal of F^- ions. All samples were tested in triplicates.

The values for different kinetic parameters were obtained via pseudo-first-order (Eq. (1)), pseudo-second-order (Eq. (2)), Elovich model (Eq. (3)) and intra-particle diffusion (Eq. (4)). The kinetic

Table 1. Different kinetic parameters of fluoride adsorption by crystal under different fluoride concentration (1.0, 3.0, and 5.0 mg L^{-1})

Kinetics equation	Parameters	Fluoride concentration (mg L^{-1})		
		1	3	5
Pseudo-First order	k_1 (mg L^{-1})	0.429	0.545	0.641
	R^2	0.944	0.928	0.917
	$q_{e\ exp}$ (mg g^{-1})	1.66	5.85	8.74
Pseudo-Second order	k_2 (g mg^{-1} min^{-1})	0.504	0.307	0.314
	R^2	0.987	0.988	0.996
	$q_{e\ cal}$ (mg g^{-1})	2.00	6.82	9.72
Intra-Particle diffusion model	k_1 (g mg^{-1} $min^{0.5}$)	0.917	3.55	4.84
	R_1^2	0.983	0.960	0.978
	k_2 (g mg^{-1} $min^{0.5}$)	0.557	1.678	1.749
	R_2^2	0.980	0.986	0.976
	k_3 (g mg^{-1} $min^{0.5}$)	0.033	0.069	0.106
	R_3^2	0.921	-	-
Elovich model	α (mg g^{-1} min^{-1})	1.94	8.76	23.61
	β (g mg^{-1})	2.15	0.660	0.527
	R^2	0.931	0.901	0.889

model that best fitted the adsorption of the crystals was explored by these values. The fitting parameter values are shown in Table 1.

$$\ln(q_e - q_t) = \ln q_e - k_1 t \quad (1)$$

$$t/q_t = 1/(k_2 q_e)^2 + t/q_e \quad (2)$$

$$q_t = \ln(\alpha\beta)/\beta + \ln t/\beta \quad (3)$$

$$q_t = k_i t^{0.5} + C_i \quad (4)$$

where q_e and q_t are the F^- adsorption quantities at equilibrium and after the time (t; min), respectively (mg/g); k_1, k_2, k_i, α, and β represent the different kinetic rate constants; C_i is a parameter used to indicate the thickness of the boundary layer.

3. Reactor Operation

To explore the most suitable environment for crystals operation, the research on the removal of Ca^{2+} and F^- was carried out in a reactor containing actual groundwater. The ANBC were added to the reactor and the operation was divided into seven phases. The effects of HRT (2 h, 4 h, and 6 h), initial Ca^{2+} concentration (0.1, 0.3, and 0.5 g L^{-1} $CaCl_2$), and pH (6.0, 7.0, and 8.0) on the removal of F^- and Ca^{2+} were investigated. The blank group was set as the control with no addition of crystals and the experimental group was loaded with the crystals.

4. Failure Response Analysis of ANBC

To evaluate the possibility of repeated recycling of materials, failure response analysis was carried out on the crystals. ANBC were operated under F^- and Ca^{2+} concentration of 4 and of 180.0 m L^{-1}, respectively. Other conditions were HRT of 6 h and pH=7. The ANBC were run 35 times repeatedly and the changes in F^- and Ca^{2+} were measured. In addition, the reactor was operated without Ca^{2+} under the same conditions to determine the removal effect. To further study the failure reaction, the SEM characterization was also performed for ANBC.

5. Analytical Techniques and Characterizations

The pH of the solution was measured with a pH meter (MM110, HACH, USA), and the F^- concentration was determined with a F^- detector equipped with a fluoride electrode (PXSJ-216F, INESA, China). The Ca^{2+} concentration was measured with flame atomic absorption spectrometry (ICP-1100, Thermo, USA) and the surface configuration of the crystals was detected by SEM (JSM-5800, JEOL, Japan). XRD (ultimate4, Rigaku, Japan) was used to investigate the composition of the crystal structure. The elemental composition of the crystals was determined by EDS (INCA Energy 350, Oxford, UK).

RESULTS AND DISCUSSION

1. Analysis of the Surface Morphology and Structure of the Crystals

Bacteria were cultured under the anaerobic conditions in a serum bottle for 24 hours at a constant temperature (30 °C) in an incubator, during which the crystals were continuously synthesized. The crystals were obtained after filtering with a vacuum pump and drying in an oven. The surface morphology of the crystals was observed with SEM. As shown in Fig. 1((a) and (b)), the crystal seeds had scattered granular distribution, different sizes, rough surfaces, complex shapes, and a variety of porous structures. The presence of bacteria had significant effects on the crystal structure [23,27]. Such a structure increased the attachment points of F^- on the seed surface, which is beneficial for the adsorption of F^- and improves the removal efficiency [5].

Fig. 1(c) shows the elemental composition in the EDS spectrum of ANBC, where C, O, Ca, and P have been detected. A typical peak of Ca appeared at 3.6 keV, indicating the formation of biocrytic seed was in the progress of MICP [18]. The typical peak of P was also detected, where P and Ca were the components of hydroxyapatite ($Ca_5(PO_4)_3(OH)$), indicating that one of the main components of Ca^{2+} precipitation was likely to be hydroxyapatite [25]. The XRD spectrum (Fig. 7) indicates the composition of the crystals and the observed diffraction peaks were mainly hydroxy-

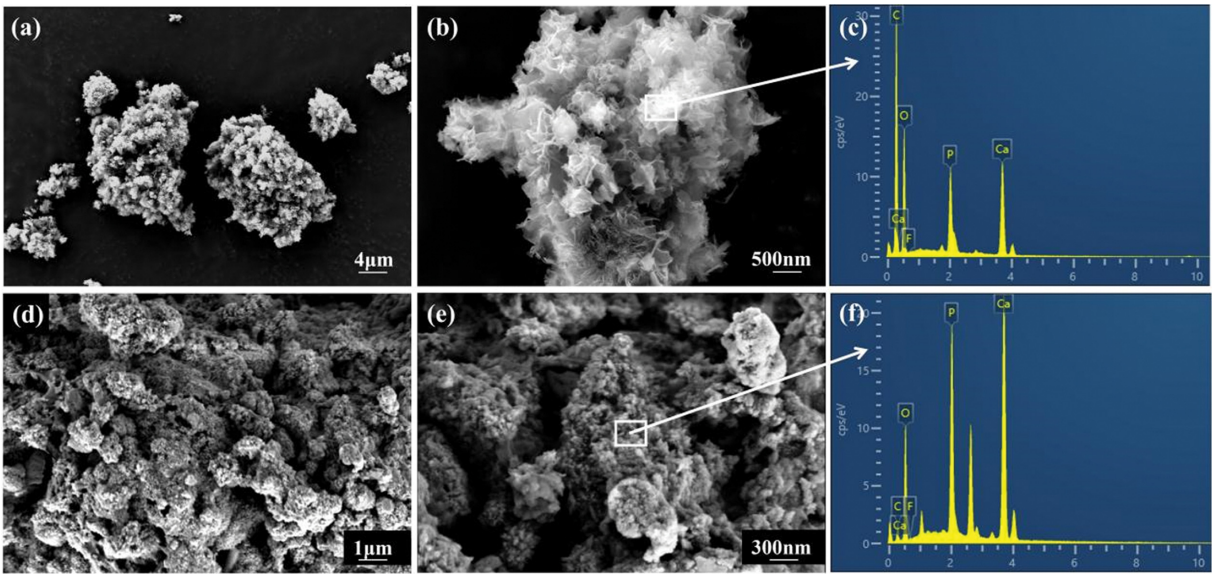

Fig. 1. SEM images (a), (b) and EDS pattern (c) of raw ANBC, SEM images (d), (e) and EDS pattern (f) of used ANBC.

apatite and calcium carbonate, which also confirmed the results of EDS.

2. Optimization of Preparation Conditions for Crystals

To achieve the best removal efficiency of the crystals, the ability of the crystals synthesized by different concentrations of F^-, Ca^{2+}, PO_4^{3-}, and Mg^{2+} was studied. Fig. 2((a) and (b)) shows that the removal efficiencies of F^- and Ca^{2+} remained almost consistent for the crystals regardless of whether F^- was added during the synthesis process. After six hours of operation, the removal efficiency of F^- was 91.16 and 93.33%, and the removal efficiency of Ca^{2+} was 64.29

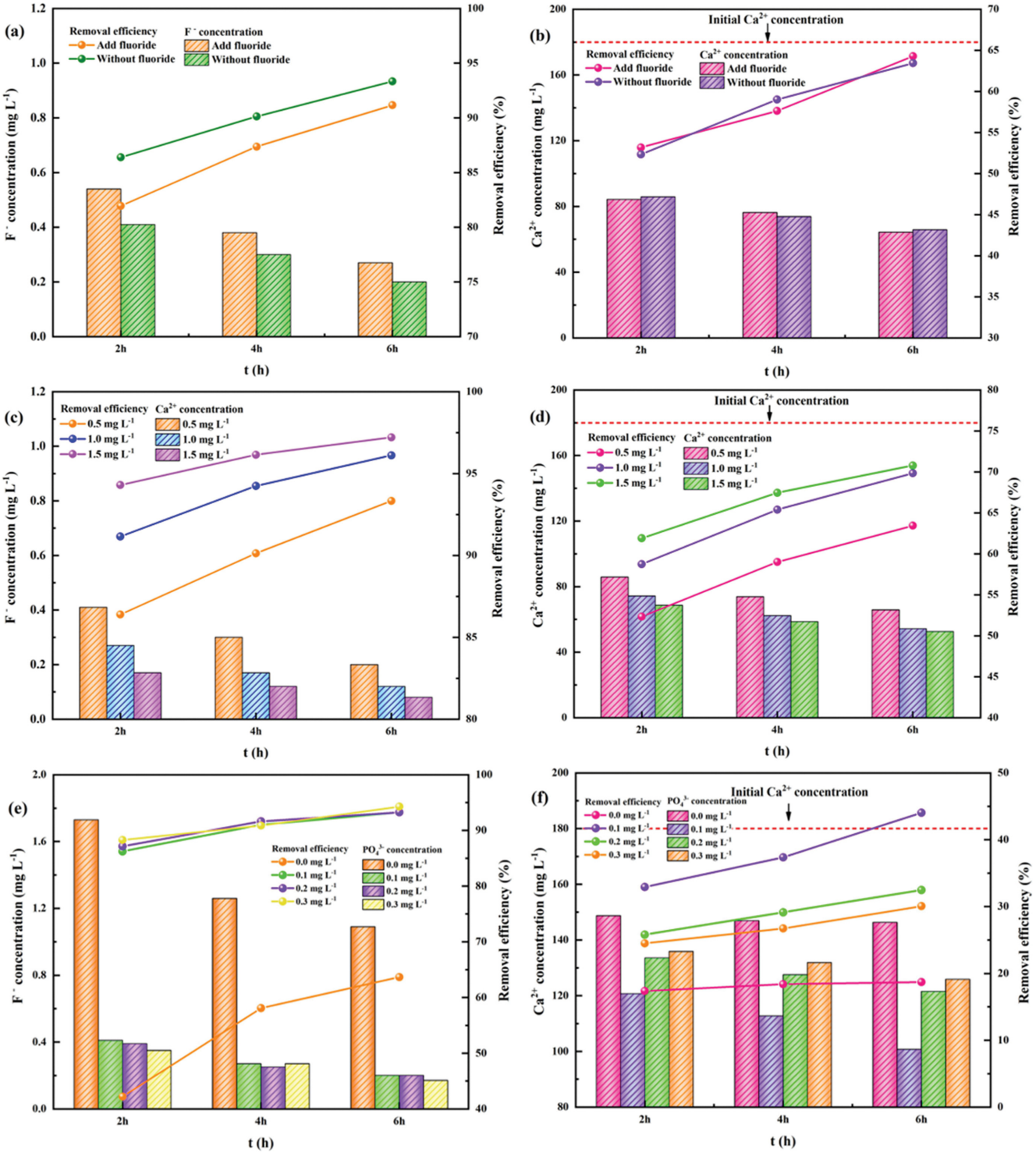

Fig. 2. F^- and Ca^{2+} removal ability of crystal prepared under different conditions: (a), (b) with and without fluoride, (c), (d) different Ca^{2+} concentration; (e), (f) different PO_4^{3-} concentration; (g), (h) different Mg^{2+} concentration; (i), (j) combined with the obtained results, synthesized under the optimal conditions.

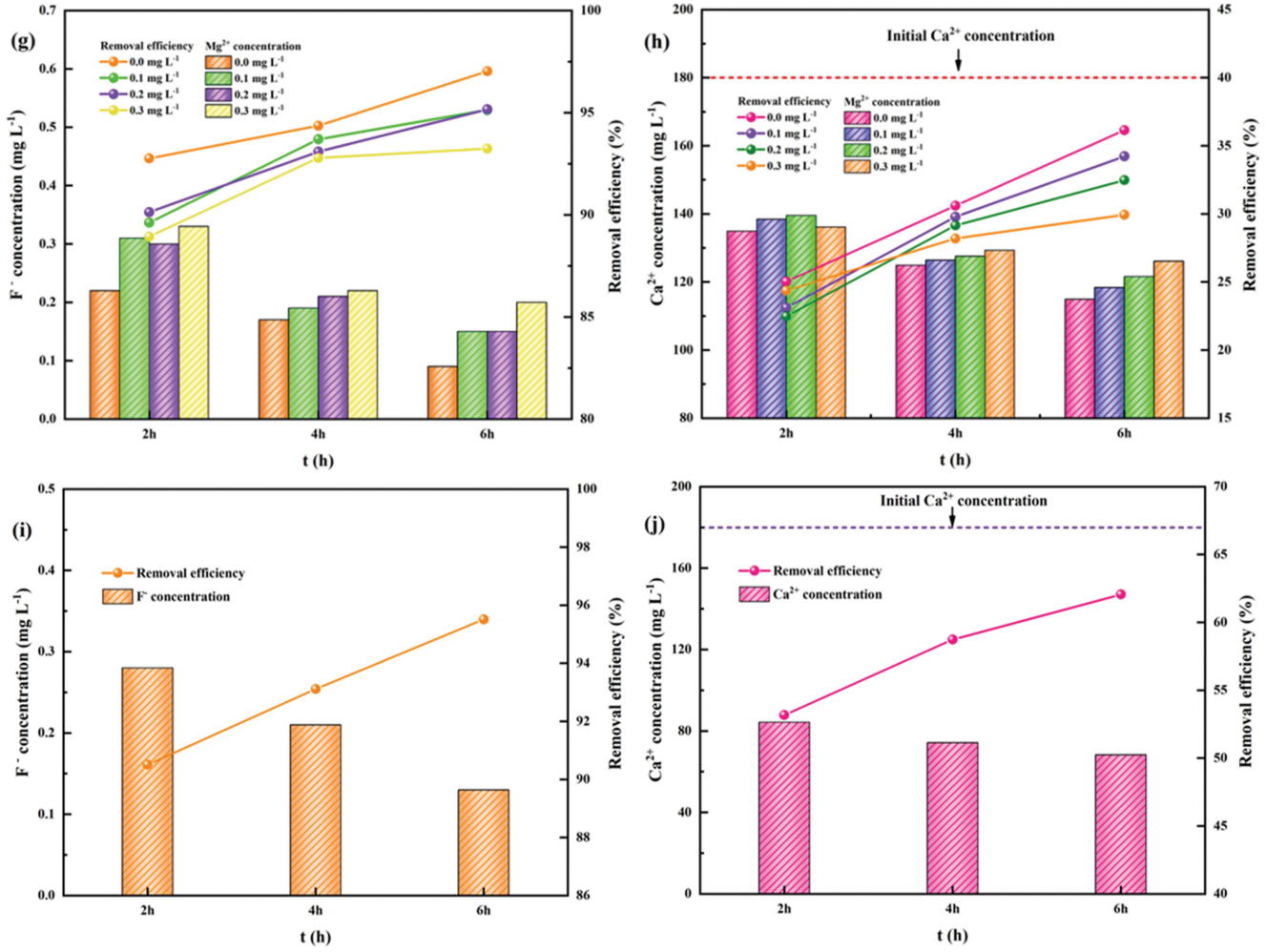

Fig. 2. Continued.

and 63.44%, indicating that the presence of F^- did not affect the effectiveness of the induced crystallization. The process of MICP can combine with F^- to form calcium fluoride phosphate ($Ca_5(PO_4)_3F$) and calcium fluoride (CaF_2) [28]. Some researchers have found that F^- and Ca^{2+} can be consistently removed from the surface of $Ca_5(PO_4)_3F$ [29]. Thus, although the addition of F^- during the preparation of the crystals resulted in the inclusion of $Ca_5(PO_4)_3F$ and CaF_2 in their composition, this did not affect the removal efficiency of F^- and Ca^{2+}.

The influence of different Ca^{2+} concentrations on crystal synthesis was studied and the effect was getting better when the Ca^{2+} concentration increased from 0.5 to 1.5 mg L^{-1}. The removal efficiency of F^- increased from 93.33 to 97.21% (Fig. 2(c)), and the removal efficiency of Ca^{2+} increased from 63.44 to 70.78% (Fig. 2(d)). Ca^{2+} is one of the main elements in the synthesis of crystals and the MICP progress [20]. When the Ca^{2+} concentration increased, the negatively charged functional groups on the surface of the bacteria attracted more Ca^{2+} [30], which increased the number of adsorption sites and improved the removal effect. When the concentration of Ca^{2+} decreased, a large amount of negatively charged functional groups cannot fully function, resulting in a decrease in the number of adsorption sites. These functional groups may be gradually destroyed by the filtration and drying processes during the preparation of the crystals, and therefore no longer have an excellent ability to bind Ca^{2+} after the crystals are synthesized, resulting in the reduced adsorption sites cannot be replenished, thus causing a decrease in the removal efficiency of F^- and Ca^{2+}.

In addition, the influence of PO_4^{3-} on synthetic crystals was investigated. The results showed that the effect was greatly improved after adding PO_4^{3-} (Fig. 2(e) and (f)). The removal efficiency of F^- and Ca^{2+} increased about 30% (from 63.67 to 94.26% and 18.71 to 44.04%, respectively). This could be due to the presence of P affecting the composition of the precipitates and calcium carbonate changes and partially converts to hydroxyapatite in a phosphate-rich environment (the latter has a lower solubility than the former) [31]. The moderate amount of hydroxyapatite plays an important role in removing F^- and Ca^{2+} [25]. However, as the amount of PO_4^{3-} increased (from 0.1 to 0.3 mg L^{-1}), the removal efficiency of Ca^{2+} significantly decreased. After 6 h of reaction, the effect was reduced by about 15%. This can be attributed to the changes in the structure of the crystals. With the increasing concentration of PO_4^{3-}, the amount of hydroxyapatite gradually increased, which greatly changed the structure of the crystals. The previous study had also shown that the morphology of hydroxyapatite was closely

related to the composition of the precursor and solution [32,33]. The changed structure was not conducive to adsorption or co-precipitation processes, thereby affecting the removal of Ca^{2+}.

Likewise, the effect of Mg^{2+} on synthetic crystals was explored. As shown in Fig. 2(g) and (h), when the concentration of Mg^{2+} increased from 0 to 0.2 mg L^{-1}, the removal efficiency of F^- and Ca^{2+} significantly decreased (from 97.03 to 93.24% and 36.15 to 29.93%, respectively), which may be due to the competitive relationship between Mg^{2+} and Ca^{2+} [34], which reduced the production of Ca^{2+} precipitation in the MICP process. When Mg^{2+} is present in the solution, the microbially induced precipitation will be partially in the form of Mg-rich calcite [35]. Mg-rich calcite can negatively affect the removal of F^- and Ca^{2+} in the system. As the concentration of Mg^{2+} in solution increases, the competition between the free Mg^{2+} in solution and the Ca^{2+} on the mineral surface becomes more intense. Since Mg^{2+} has a stronger affinity for certain sites on the mineral surface, Mg^{2+} can gradually replace part of the Ca^{2+} [36], thus affecting the removal of F^- and Ca^{2+} from the crystals.

Combining the influence of these factors and taking into account the economic factors, the optimal preparation and culture conditions of crystals were determined, i.e., Ca^{2+} was 1.0 mg L^{-1}, PO_4^{3-} was 0.1 mg L^{-1}, and Mg was 0.0 mg L^{-1}, and the effect of crystals prepared under these conditions was investigated. After 6 hours of experimental operation, the removal efficiency of F^- and Ca^{2+} reached 95.51 and 62.06% (Fig. 2(i) and (j)), respectively, indicating that the effect of the crystals prepared under these conditions is reliable.

3. Adsorption Kinetics and Velocity Control Mechanism

Adsorption experiments under three F^- concentrations (1, 3, and 5 mg L^{-1}) were carried out, the pH was set to 7.0 and the amount of crystals was 0.5 g L^{-1}. Four well-known adsorption kinetic models were employed. The fitting results and a series of parameter values are shown in Fig. 3 and Table 1. According to Fig. 3((a) and (b)), it can be seen that the adsorption of the crystals was in line with the pseudo-second-order model and its correlation coefficient (R^2) could reach 0.987, 0.988, and 0.996, which is significantly better than the pseudo-first-order model (0.944, 0.928, and 0.917, respectively) (Table 1). In addition, the q_e (experimental value) is very close to the q_e (calculated value) of the pseudo-second-order kinetic model. Therefore, the dominant role in the entire adsorption process is chemical adsorption [37,38] and the rate-limiting step is related to the valency forces of sharing or exchanging electrons [39].

According to Fig. 3(b), the F^- concentrations of 3.0 and 5.0 mg L^{-1} were better fitted than 1.0 mg L^{-1} and the data in Table 1 also

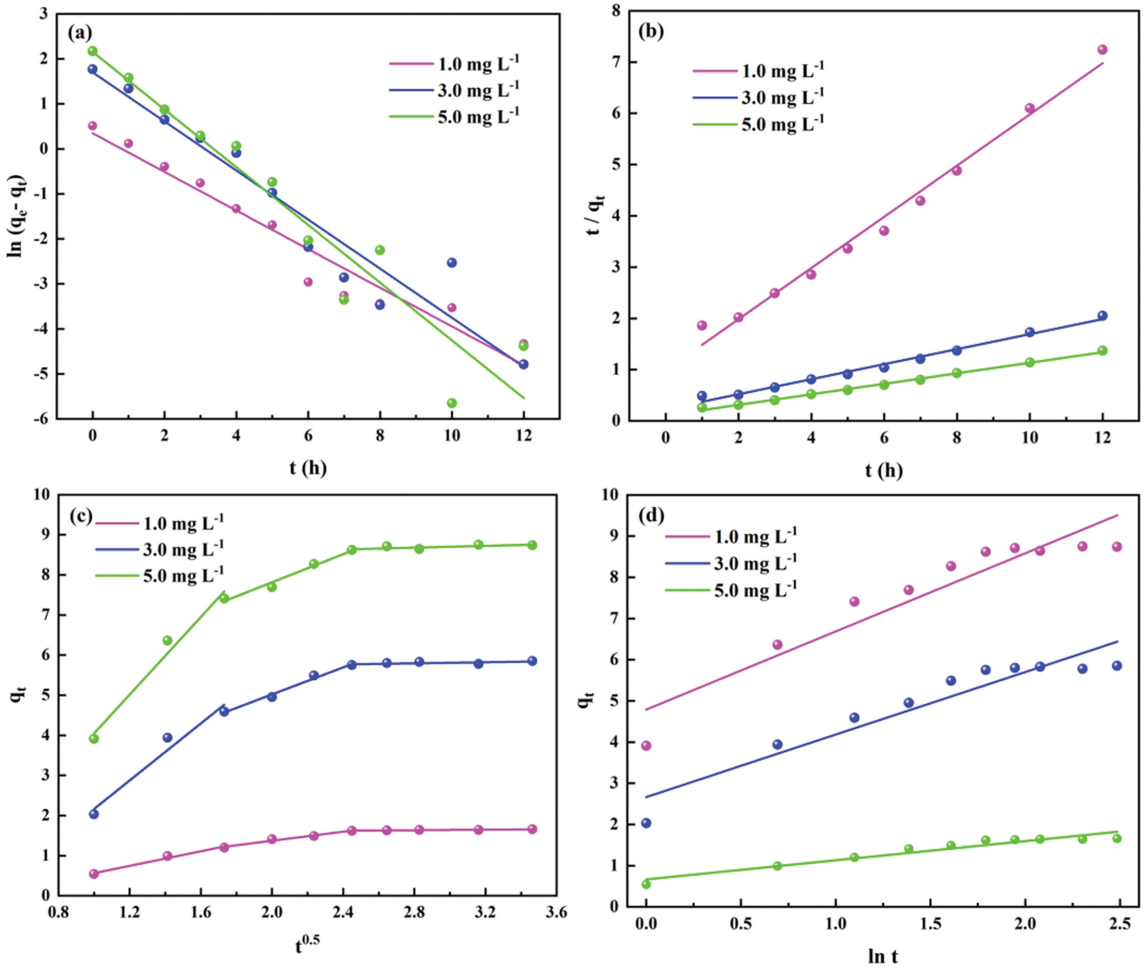

Fig. 3. Kinetic analysis under different fluoride concentration: (a) Pseudo-first order model, (b) Pseudo-second order model, (c) Intra-particle diffusion model, (d) Elovich model.

supported these results. When the initial F^- concentration increased from 1.0 to 3.0 mg L^{-1}, the reaction rate constant k_2 in the pseudo-second-order model decreased from 0.50 to 0.30, indicating that when the dosage of crystals was constant, too high F^- concentrations can restrict the adsorption rate [39]. This is due to the immobilization of more F^- ions by the crystals and the lack of active adsorption sites [40,41]. When the concentration increased from 3.0 to 5.0 mg L^{-1}, k_2 was the same (from 0.30 to 0.31). It indicated that the F^- concentration of 3.0 mg L^{-1} may be the limiting value of defluoridation at the crystal dosage of 0.5 g L^{-1}.

The Intra-particle diffusion model was used to analyze the control steps of the reaction process. As shown in Fig. 3(c), three phases of the adsorption process can be seen and the equations fitted in each system did not pass the origin. A multi-linear graph is displayed, indicating that the intra-particle diffusion was not the only part of this process [42]. Boundary layer diffusion affected the adsorption process to a certain extent [43] and the adsorbent was multiphase and multiple simultaneous processes controlled the entire adsorption [42]. When the initial concentration of F^- changed, the general trend of the intra-particle diffusion model remained unchanged, the adsorption capacity began to increase rapidly and then the increase rate slowed until stability. This shows that at the beginning there were abundant binding sites on the surface of the crystals and a large amount of F^- was adsorbed on it. At the same time, F^- entered the free channel inside the crystals and the adsorption efficiency was rapidly increased. This process was mainly controlled by external mass transfer and intra-particle diffusion or pore diffusion [43]. As the adsorption proceeded, the surface binding sites and internal free channels were gradually occupied, gradually slowing adsorption efficiency, and this process also hindered the progress of diffusion [41]. Gradually, the adsorption reached equilibrium and intra-particle diffusion was no longer the control step [44].

The Elovich model is an empirical formula that contains a series of adsorption reaction mechanisms in the solid-liquid interface. It is mainly suitable for the heterogeneous diffusion adsorption process dominated by chemical adsorption [45]. The fitting effect of the Elovich model established in this experiment (Fig. 3(d)) was not as good as the pseudo-first-order and pseudo-second-order models; the R^2 can still reach about 90%. To some extent, this further shows that chemical adsorption dominated the entire adsorption process [46]. Ion exchange exists during the adsorption process [47].

4. The Effects of HRT, Initial Ca^{2+} Concentration, and pH on ANBC

The removal characteristics of F^- and Ca^{2+} in the reactor under different HRT conditions were investigated. In stages 1-3, the HRT was 2, 4, and 6 h, and other conditions remained the same (pH was 7.0 and the influent F^- and Ca^{2+} concentrations were 4.0 and 180.0 mg L^{-1}, respectively). Fig. 4 shows that the maximum removal efficiency of F^- in groundwater by the crystals could reach 93.31% when the HRT was 6 h, which is significantly higher than 2 and 4 h (74.53 and 80.88%, respectively). At the same time, the removal efficiency of Ca^{2+} could reach 66.20%, which was higher than 2 and 4 h (50.90 and 57.20%, respectively). The full contact between F^-, Ca^{2+}, and crystals was the key to improving the effect [13]. With the extension of the reaction time, the contact time between ions and crystals also increased, thus increasing the removal rate [26, 48]. It can be seen that ANBC can achieve an excellent F^- and Ca^{2+} removal effect in a short time, which provides the possibility for practical engineering applications.

Stages 3-5 explored the effect of pH on the crystals. The corresponding pH of each stage was 7.0, 6.0, and 8.0 and the other conditions remained the same (the HRT was 6 h and the influent F^- and Ca^{2+} concentrations were 4.0 and 180.0 mg L^{-1}, respectively). As shown in Fig. 4, the maximum removal efficiency was at pH= 7.0 and the removal efficiency of F^- and Ca^{2+} was 93.31 and 63.20%, respectively. When the pH was 8.0, the maximum F^- and Ca^{2+} removal efficiency was 65.41 and 54.60%, respectively. Moreover, when the pH was 6.0, the maximum F^- and Ca^{2+} removal efficiency was 85.66 and 63.00%, respectively. It can be seen that when the environment was weakly alkaline, the F^- removal efficiency dropped sharply. This could be attributed to the fact that when the pH rises from neutral to alkaline, the surface of the crystals is negatively charged, and the Coulomb repulsion between the negatively charged surface and the F^- in the solution causes the adsorption of F^- to decrease significantly [49,50]. Both showed efficient F^- removal effects at pH=6.0 and 7.0. This can be explained that when the pH is low, the surface of the seed crystals is positively charged, which is beneficial to enhance the adsorption of negatively charged F^- [49]. To avoid crystals failure, the removal effect at higher or lower pH was not explored and pH=7.0 was set as the optimal pH value for the subsequent experiment.

Similarly, the effect of initial Ca^{2+} concentration was studied. In stages 3, 7, and 6, the initial Ca^{2+} concentration was set to 180.0, 108.0, and 36.0 mg L^{-1}. The HRT was set at 6 h and the pH was 7.0. The influent F^- concentration was 4.0 mg L^{-1}. As shown in Fig. 4, when the concentration of Ca^{2+} increased from 36.0 to 180.0 mg L^{-1}, the removal efficiency of F^- increased from 71.91 to 93.31%, respectively, indicating that the external Ca^{2+} supplementation has a positive effect on the removal of F^-. In addition, with the increase of the initial Ca^{2+} concentration, although the removal rate of Ca^{2+} did not change much, the maximum removal amount increased from 26.2 to 74.3 mg L^{-1}, and then to 121.8 mg L^{-1}. Since the initial Ca^{2+} concentration is quite different, it is more meaningful to consider the amount of removal. Therefore, the removal effect increased as the Ca^{2+} concentration increased, which showed a good correlation with the removal of the F^-. It could be explained that during the formation of the crystals, a large amount of negatively charged EPS would be produced [22]. These negative groups in EPS could attract Ca^{2+} to form a stable complex [51]. The higher the concentration of Ca^{2+}, the more Ca^{2+} containing complexes were produced and more F^- was removed [52]. Furthermore, the solubility product principle can also be used to explain this phenomenon. According to this principle, when the concentration of Ca^{2+} in water increased, it was easier to reach the K_{sp} of calcite ($CaCO_3$), hydroxyapatite ($Ca_5(PO_4)_3OH$), and $Ca_5(PO_4)_3F$ precipitation [53]. As a F^- adsorbent, the accumulation of $Ca_5(PO_4)_3OH$ was more conducive to the removal of F^- [54]. The removal efficiency of F^- and Ca^{2+} in the control group without ANBC did not change significantly, with an average of 4.75 and 3.52%, respectively.

5. Failure Response Analysis of ANBC

Repeated utilization performance is an important indicator for

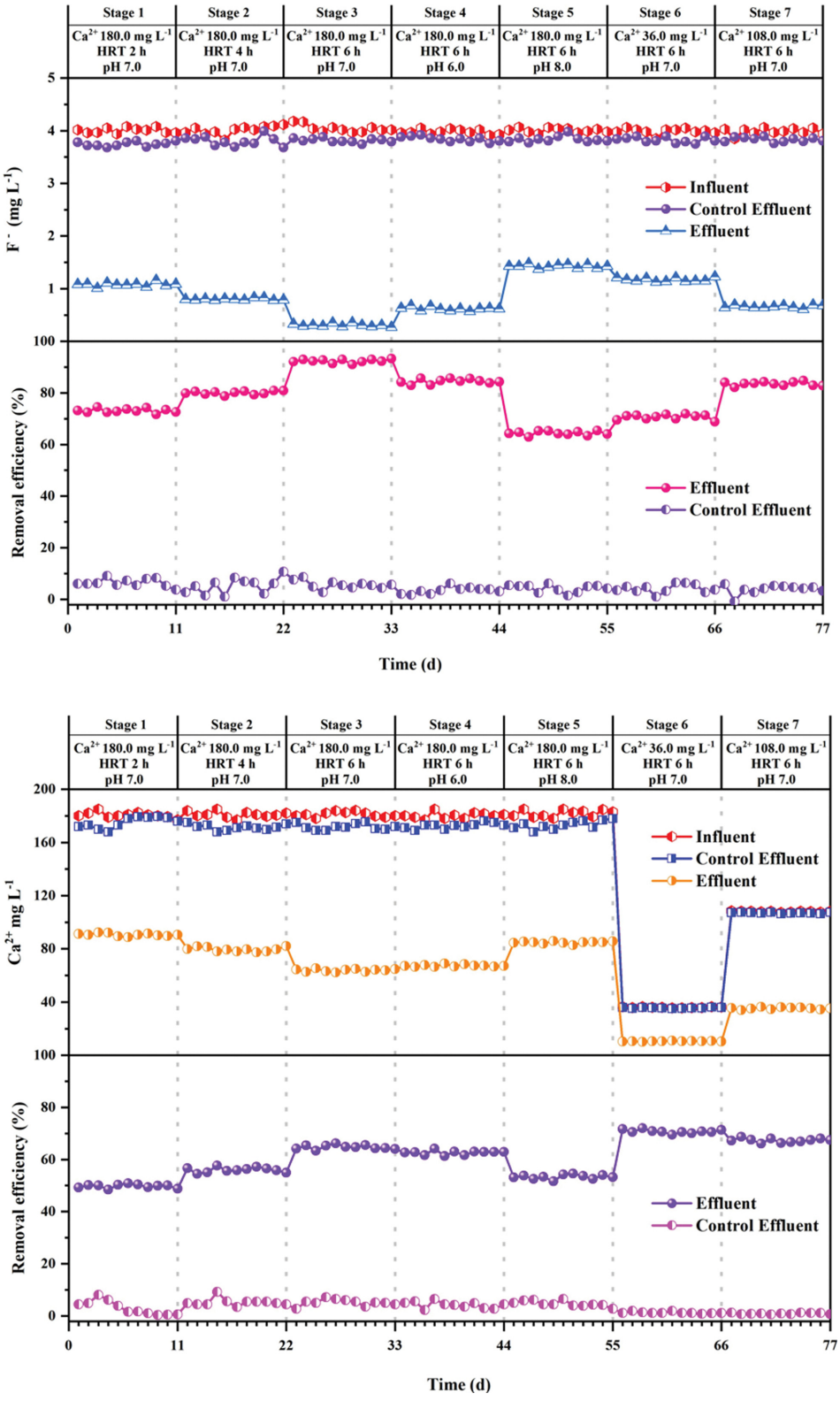

Fig. 4. The effect of HRT, pH, and initial Ca^{2+} concentration on the performance of ANBC reactor at the 7 operational periods.

evaluating the quality of materials [6]. As shown in Fig. 5(a) and (b), under the conditions of F^- and Ca^{2+} concentration of 4 and 180 mg L^{-1}, respectively, HRT of 6 h, pH of 7.0, ANBC still maintained an efficient removal rate after 35 consecutive runs (89.85 and 59.86% for F^- and Ca^{2+}, respectively). During this period, the removal efficiency fluctuated very little (maintained above 85 and 55% for F^- and Ca^{2+}, respectively), indicating that the crystals could be repeatedly used. These are interesting results obtained in this

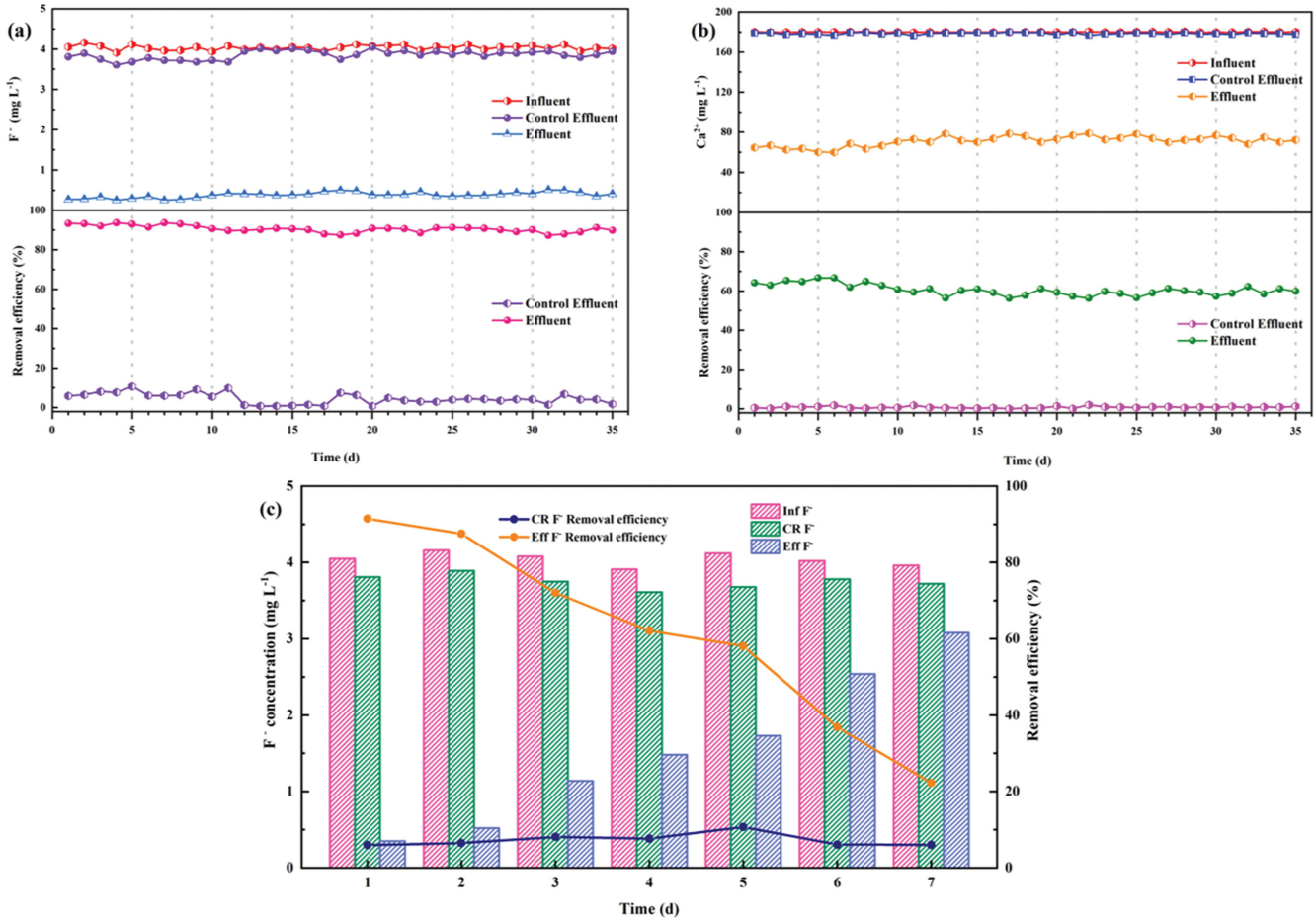

Fig. 5. Repeated utilization performance of ANBC: (a), (b) removal efficiency of F^- and Ca^{2+} by the crystal in 35 times of repeated use; (c) the efficiency without adding Ca^{2+}.

study. Theoretically, the effective sites of the crystals will continue to be occupied during the adsorption process and the adsorption capacity will become weaker [55]. It is speculated that the recycling of ANBC may be related to its continuous formation. For this reason, the reuse of ANBC was carried out without adding Ca^{2+} under the same conditions. The results show that the removal efficiency of F^- significantly decreased. After the seventh operation, the F^- removal rate dropped to 22.25% (Fig. 5(c)) and the crystals were saturated. Due to the limited adsorption sites, each use was accompanied by its occupation and the lack of Ca^{2+} prevented the crystals from continuing growth, which led to its saturation. The SEM image further showed the failure process. According to the comparison before and after the crystal's saturation, it was found that the crystals after saturation were tightly wrapped and it was difficult to find the vacant sites (Fig. 6(c) and (d)); while the crystals before saturation could always find a large number of empty sites (Fig. 6(a) and (b)). Thus, renewal growth played a decisive role in the removal process. In addition, the continuous steady removal effect indicated that ANBC renewed and grew rapidly; therefore, it has great potential in practical engineering applications.

6. Mechanism of ANBC for Fluoride and Calcium Removal

To further study the mechanism of F^- and Ca^{2+} removal by ANBC, the SEM, EDS, and XRD were used for characterization and analyses. By observing the SEM image of the crystals, it showed that the size of the crystals was different and full of pores (Fig. 1(a) and (b)), indicating that small crystals of different diameters will continue to gather during the growth of the crystals [16]. Wimalasiri et al. [56] also discovered that nanohydroxyapatite aggregated together in the form of rod-like or spherical particles, forming a wide range of pores. Among them, the bacteria are in the core position; by inducing Ca^{2+} precipitation to form the crystals skeleton [57] and continuously producing viscous secretions in this process will promote the aggregation of the crystals to a certain extent [19].

By comparing the images before and after the defluoridation of ANBC, it was found that the surface of the crystals after the action became rough and much particulate matter was attached (Fig. 1(d)). A higher magnification image showed that the original sheet structure of the crystals became spherical and the edges and corners were no longer distinct (Fig. 1(e)). A large amount of F^- and Ca^{2+} was removed after the crystals were put into the water body, indicating that the surface of the crystals was covered by abundant F^- and Ca^{2+}. The surface of the material became rougher after use as was also reported by other researchers, and the initial complex structure was the key to the function of the crystals [39,58].

The EDS results showed that the main elements of the original

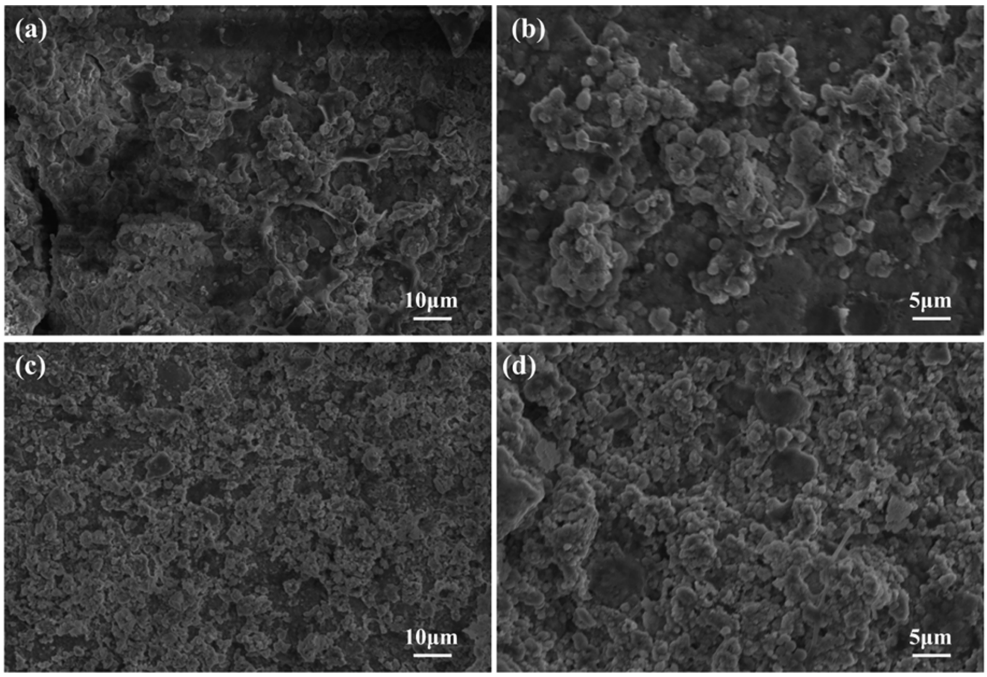

Fig. 6. SEM images before and after ANBC failure: (a), (b) before and (c), (d) after.

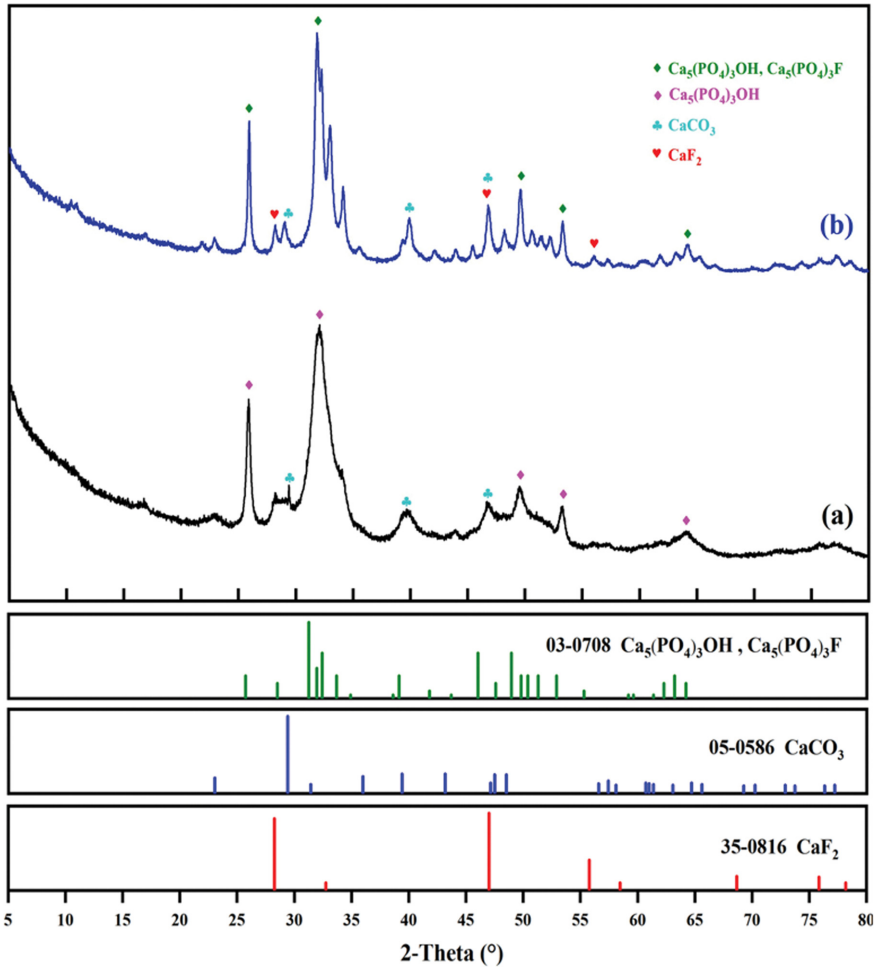

Fig. 7. Peak spectra of raw ANBC (a) and used ANBC (b) by XRD.

crystals were C, O, P, and Ca, and the atomic percentages were 66.34, 27.43, 2.12, and 4.11%, respectively (Fig. 1(c)). While the atomic percentages of C, O, P, and Ca in the crystals after the action were 17.08, 52.09, 10.45, and 19.83%, respectively (Fig. 1(f)). In addition, 0.55% of F^- was also detected, confirming the F^- removal ability of the crystals. The increase in P and O elements indicated that PO_4^{3-} was involved in the growth of the crystals and the increase in Ca was the result of the occurrence of Ca^{2+} in the environment on the surface of the crystals in various forms [59].

XRD further indicated the composition of the crystals before and after its effect. As shown in Fig. 7, the main components before adsorption were $Ca_5(PO_4)_3OH$ and $CaCO_3$. The diffraction peaks at 25.9°, 32.0°, 49.6°, 53.2°, and 64.0° were attributed to $Ca_5(PO_4)_3OH$ and the peaks at 29.4°, 39.7°, and 46.7° corresponded to $CaCO_3$. After crystallization, the main components were CaF_2, $Ca_5(PO_4)_3F$, and $CaCO_3$. The formation of CaF_2 was detected at the peaks of 28.2°, 46.8°, and 56.0°, indicating that the nucleation sites on crystals binding to F^- in solution were one of the main mechanisms of F^- removal [33]. Earlier, a few researchers also found that F^- could combine with Ca^{2+} in calcite to form CaF_2 [10]. Alternatively, $Ca_5(PO_4)_3OH$ can also generate $Ca_5(PO_4)_3F$ after adsorbing F^-, which will largely be removed in the form of $Ca_5(PO_4)_3F$ [60,61]. These results were also consistent with the analysis of the EDS.

Based on our findings, the main mechanisms of defluoridation by ANBC were proposed as: (i) $CaCO_3$ on the surface of the crystals chemically adsorbed F^- through ion exchange and F^- is fixed to the crystals in the form of CaF_2, (ii) The hydroxyl group in $Ca_5(PO_4)_3OH$ is replaced by F^-, converted from $Ca_5(PO_4)_3OH$ to $Ca_5(PO_4)_3F$, (iii) Free Ca^{2+}, F^-, and PO_4^{3-} are co-precipitated to form $Ca_5(PO_4)_3F$ and CaF_2, in which the addition of the crystals facilitated this process [54,61]. These reactions can be represented by the chemical formulae:

(1) $ANBC\text{-}CaCO_3+2F^-+H^+=ANBC\text{-}CaF_2+HCO_3^-$

(2) $ANBC\text{-}Ca_5(PO_4)_3OH+F^-=ANBC\text{-}Ca_5(PO_4)_3F+OH^-$

(3) $5Ca^{2+}+F^-+3PO_4^{3-}=Ca_5(PO_4)_3F$

(4) $Ca^{2+}+2F^-=CaF_2$

CONCLUSIONS

The application of ANBC in groundwater remediation was evaluated. The result showed that ANBC can remove up to 93.31 and 66.2% of F^- and Ca^{2+} within 6 hours, respectively. Therefore, it can be used as an ideal medium for groundwater remediation. The adsorption kinetics showed that the removal of F^- by ANBC was multi-layer heterogeneous adsorption dominated by chemical adsorption. The optimal preparation conditions of ANBC (1.0 mg L^{-1} Ca^{2+}, 0.1 mg L^{-1} PO_4^{3-}, and 0.0 mg L^{-1} Mg^{2+}) and reactor operating conditions (6 h HRT, pH=7.0, and 180 mg L^{-1} Ca^{2+}) were determined. The crystal failure reaction showed that the reuse of crystals was related to continuous crystal formation and high removal ability was maintained after 35 repetitions. The SEM, EDS, and XRD further revealed the F^- removal mechanism of ANBC, which was mainly manifested by the adsorption of F^- and the co-precipitation between Ca^{2+}, F^-, and PO_4^{3-}. As a new low-cost F^- removal medium, especially with long-term stability, ANBC has high practical value and provides a new choice for the removal of F^- and Ca^{2+} from groundwater.

ACKNOWLEDGEMENTS

This research work was partly supported by the National Natural Science Foundation of China (NSFC; No. 51978556 and No. 51678471), Shaanxi Science Fund for Distinguished Young Scholars, China (No. 2019JC-31), and the Youth Innovation Team Construction Scientific Research Project of Shaanxi Education Department (No. 21JP064).

DECLARATION OF INTERESTS

The authors declare that they have no known competing financial interests or personal relationships that could have appeared to influence the work reported in this paper.

REFERENCES

1. P. K. Jha and P. Tripathi, *Groundw. Sustain. Dev.*, **13**, 100576 (2021).
2. N. AL-Darwish and T. M. Abu-Sharar, *Appl. Water Sci.*, **11**(2), 37 (2021).
3. Y. Li, Y. H. Bi, W. J. Mi, S. L. Xie and L. Ji, *J. Hazard. Mater.*, **406**, 124337 (2021).
4. H. Su, W. D. Kang, Y. R. Li and Z. Li, *Environ. Pollut.*, **286**, 117287 (2021).
5. D. E. Jayashree, P. S. Kumar, P. T. Ngueagni, D. V. Vo and K. W. Chew, *Environ. Pollut.*, **272**, 115969 (2021).
6. X. Borgohain, A. Boruah, G. K. Sarma and H. Rashid, *J. Mol. Liq.*, **305**, 112799 (2020).
7. C. F. Z. Lacson, M. C. Lu and Y. H. Huang, *J. Cleaner Prod.*, **280**, 124236 (2021).
8. K. K. Yadav, S. Kumar, Q. B. Pham, N. Gupta, S. Rezania, H. Kamyab, S. Yadav, J. Vymazal, V. Kumar, D. Q. Tri, A. Talaiekhozani, S. Prasad, L. M. Reece, N. Singh, P. K. Maurya and J. Cho, *Ecotoxicol. Environ. Saf.*, **182**, 109362 (2019).
9. X. Y. Wang, J. J. Wei, W. C. Peng, J. M. Dan, J. Y. Wang and J. L. Zhang, *Appl. Surf. Sci.*, **552**, 149423 (2021).
10. J. I. Lee, J. K. Kang, S. H. Hong, C. G. Lee, S. Jeong and S. J. Park, *Chemosphere*, **263**, 128328 (2021).
11. J. Y. He, Y. Yang, Z. J. Wu, C. Xie, K. S. Zhang, L. T. Kong and J. H. Liu, *J. Environ. Chem. Eng.*, **8**, 104516 (2020).
12. S. Shao, B. Z. Ma, Y. Q. Chen, W. J. Zhang and C. Y. Wang, *Chem. Eng. J.*, **426**, 131364 (2021).
13. M. Sadhu, P. Bhattacharya, M. Vithanage and P. P. Sudhakar, *Sep. Purif. Technol.*, **278**, 119106 (2022).
14. D. W. Cho, Y. S. Han, J. Lee, J. Y. Jang, G. J. Yim, S. Cho, J. S. Lee and Y. W. Cheong, *Chemosphere*, **247**, 125899 (2020).
15. K. S. D. Premarathna, A. U. Rajapaksha, B. Sarkar, E. E. Kwon, A. Bhatnagar, Y. S. Ok and M. Vithanage, *Chem. Eng. J.*, **372**, 536 (2019).
16. A. Rajasekar, S. Wilkinson and C. K. S. Moy, *Environ. Sci. Ecotechnol.*, **6**, 100096 (2021).
17. Z. Wang, J. F. Su, A. Ali, R. J. Zhang, W. S. Yang, L. Xu, J. Shi and Z. H. Gao, *Sci. Total Environ.*, **806**, 150341 (2022).
18. S. G. Choi, I. Chang, M. Lee, J. H. Lee, J. T. Han and T. H. Kwon,

Constr. Build. Mater., **246**, 118415 (2020).
19. W. Qin, C. Y. Wang, Y. X. Ma, M. J. Shen, J. Li, K. Jiao, F. R. Tay and L. N. Niu, *Adv. Mater.*, **32**(22), 1907833 (2020).
20. M. Naveed, J. G. Duan, S. Uddin, M. Suleman, Y. Hui and H. Li, *Ecol. Eng.*, **153**, 105885 (2020).
21. P. P. Xu, H. Fan, L. J. Leng, L. L. Fan, S. H. Liu, P. Chen and W. G. Zhou, *Algal Res.*, **47**, 101831 (2020).
22. S. Y. Qiao, G. Q. Zeng, X. T. Wang, C. G. Dai, M. P. Sheng, Q. Chen, F. Xu and H. Xu, *Chemosphere*, **274**, 129661 (2021).
23. X. Chen, D. Zhang, S. L. Larson, J. H. Ballard, H. M. Knotek-Smith, J. Nie, N. Hu, D. X. Ding and F. X. X. Han, *Water, Air, Soil Pollut.*, **232**(7), 268 (2021).
24. G. S. Zeng, B. Ling, Z. J. Li, S. L. Luo, X. Z. Sui and Q. Guan, *J. Hazard. Mater.*, **373**, 313 (2019).
25. J. R. Liu, J. F. Su, A. Ali, Z. Wang and R. J. Zhang, *J. Hazard. Mater.*, **423**, 126976 (2022).
26. Y. Y. Fan, J. F. Su, Z. Wang, L. Y. Deng and H. Zhang, *Chemosphere*, **273**, 129667 (2021).
27. A. Ansari, J. Pena-Bahamonde, S. K. Fanourakis, Y. D. Hu and D. F. Rodrigues, *Water Res.*, **179**, 115863 (2020).
28. J. F. Su, R. J. Zhang, X. F. Hu, A. Ali and Z. Wang, *Korean J. Chem. Eng.*, **39**(3), 665 (2022).
29. L. Y. Deng, Y. Wang, J. Q. Zhou, T. L. Huang and X. Sun, *J. Ind. Eng. Chem.*, **83**, 35 (2020).
30. M. J. Chen, Y. F. Li, X. R. Jiang, D. R. Zhao, X. F. Liu, J. L. Zhou, Z. F. He, C. L. Zheng and X. L. Pan, *J. Hazard. Mater.*, **411**, 125103 (2021).
31. M. L. Wang, S. J. Wu, J. A. Guo, Z. S. Liao, Y. Q. Yang, F. R. Chen and R. L. Zhu, *J. Hazard. Mater.*, **412**, 125261 (2021).
32. J. Prywer and M. Olszynski, *J. Cryst. Growth*, **375**, 108 (2013).
33. Z. Wang, J. F. Su, X. F. Hu, A. Ali and Z. Z. Wu, *J. Hazard. Mater.*, **406**, 124748 (2021).
34. N. Borner, B. D. Baere, L. G. Akita, R. Francois, K. P. Jochum, P. Frenzel, L. P. Zhu and A. Schwalb, *J. Paleolimnol.*, **58**, 191 (2017).
35. H. X. Yan, Z. Z. Han, H. Zhao, J. T. Pan, Y. H. Zhao, M. E. Tucker, J. X. Zhou, X. Y. Yan, H. Y. Yang and D. Fan, *J. Cleaner Prod.*, **252**, 119826 (2020).
36. J. Paquette and R. J. Reeder, *Geochim. Cosmochim. Acta*, **59**(4), 735 (1995).
37. R. Shahrokhi-Shahraki, C. Benally, M. G. El-Din and J. Park, *Chemosphere*, **264**, 128455 (2021).
38. M. Gao, W. Wang, H. B. Yang and B. C. Ye, *Micropor. Mesopor. Mater.*, **289**, 109620 (2019).
39. U. Kumari, S. K. Behera, H. Siddiqi and B. C. Meikap, *J. Hazard. Mater.*, **381**, 120917 (2020).
40. M. B. Baskan and A. R. Biyikli, *Water Environ. Res.*, **93**(4), 620 (2021).
41. A. Mullick and S. Neogi, *Ultrason. Sonochem.*, **50**, 126 (2019).
42. A. Saini, S. S. Tripathy, P. H. Maheshwari and S. R. Dhakate, *Mater. Res. Express.*, **6**(8), 085605 (2019).
43. M. Kim, C. E. Choong, S. Hyun, C. M. Park and G. Lee, *Chemosphere*, **253**, 126580 (2020).
44. X. Hu, H. Zhang and Z. R. Sun, *Appl. Surf. Sci.*, **392**, 332 (2017).
45. S. H. Chien and W. R. Clayton, *Soil Sci. Soc. Am. J.*, **44**(2), 265 (1980).
46. S. S. A. Alkurdi, R. A. Al-Juboori, J. Bundschuh, L. Bowtell and A. Marchuk, *J. Hazard. Mater.*, **405**, 124112 (2021).
47. M. Y. Han, J. H. Zhang, Y. Y. Hu and R. P. Han, *J. Chem. Eng. Data*, **64**, 3641 (2019).
48. Y. H. Bai, J. F. Su, A. Ali, Q. Wen, Q. Chang, Z. H. Gao and Y. Wang, *Bioresour. Technol.*, **344**, 126228 (2022).
49. F. H. Li, J. Jin, Z. Y. Shen, H. S. Ji, M. Yang and Y. M. Yin, *J. Hazard. Mater.*, **388**, 121734 (2020).
50. C. L. Chen, S. W. Park, J. F. Su, Y. H. Yu, J. E. Heo, K. D. Kim and C. P. Huang, *Sci. Total Environ.*, **693**, 133605 (2019).
51. H. Q. Yu, J. H. Tay and H. H. P Fang, *Water Res.*, **35**(4), 1052 (2001).
52. S. Gogoi, S. K. Nath, S. Bordoloi and R. K. Dutta, *J. Environ. Manage.*, **152**, 132 (2015).
53. P. Anbu, C. H. Kang, Y. J. Shin and J. S. So, *SpringerPlus*, **5**(1), 250 (2016).
54. J. R. Liu, A. Ali, J. F. Su, Z. Z. Wu, R. J. Zhang and R. B. Xiong, *J. Hazard. Mater.*, **416**, 125776 (2021).
55. K. Mukhopadhyay, A. Naskar, U. C. Ghosh and P. Sasikumar, *J. Hazard. Mater.*, **384**, 121235 (2020).
56. A. K. D. V. K. Wimalasiri, M. S. Fernando, G. R. Williams, D. P. Dissanayake, K. M. N. de Silva and R. M. de Silva, *Mater. Chem. Phys.*, **257**, 123712 (2021).
57. L. Ma, A. P. Pang, Y. S. Luo, X. L. Lu and F. M. Lin, *Microb. Cell Fact.*, **19**(1), 12 (2020).
58. S. Zhang, A. Ali, J. F. Su, T. L. Hung and M. Li, *Water Res.*, **209**, 117899 (2022).
59. S. Sepulveda, C. Duarte-Nass, M. Rivas, L. Azocar, A. Ramirez, J. Toledo-Alarcon, L. Gutierrez, D. Jeison and A. Torres-Aravena, *Minerals*, **11**(8), 905 (2021).
60. T. Miyazaki and S. Muroyama, *Ceram. Int.*, **47**, 16225 (2021).
61. A. Ali, Z. Wu, M. Li and J. Su, *Bioresour. Technol.*, **333**, 125154 (2021).